Supplementary information for "Numerical-experimental observation of shape bistability of red blood cells flowing in a microchannel"

Achim Guckenberger,[a] Alexander Kihm,[b] Thomas John,[b] Christian Wagner,[b c] Stephan Gekle[a]

Dated: January 22, 2018

Contents

S1 About the initial condition

S1.1 Croissant and slipper initial shapes

Figure S1 shows the employed red blood cell (RBC) shapes when the initial shape is taken to be a croissant or slipper. These shapes were obtained from previous simulations where we started with the typical discocyte shape[1] whose axis was aligned with the channel's axis (see figure 2 in the main text). On the one hand, the croissant shape was extracted from a converged simulation where the initial radial offset was 0.17 µm and the steady state cell velocity was 6.61 mm/s. The ellipsoidal rim of the croissant has a diameter ranging from 6.0 µm to 6.6 µm. Moreover, the total length of the cell (rim to tip) is 6.7 µm, while the distance from the dent to the tip is 4.4 µm. On the other hand, the slipper was retrieved from a simulation with an initial radial offset of 0.86 µm, with the average cell velocity in the steady state being 6.48 mm/s. The slipper has a total length of 9.7 µm, a height (y-extent) of 4.0 µm and a width (z-extent) of 6.2 µm. We chose a frame in the middle of the periodic contraction/expansion of the cell. Hence, these two shapes correspond to two simulations from figure 5 in the main text. The slightly different velocities come from the fact that at otherwise identical flow

[a]Biofluid Simulation and Modeling, Fachbereich Physik, Universität Bayreuth, Bayreuth
[b]Experimental Physics, Saarland University, 66123, Saarbrücken, Germany
[c]Physics and Materials Science Research Unit, University of Luxembourg, Luxembourg, Luxembourg

[1]For the formula of the typical discocyte shape see references [1, 2].

parameters croissants are faster than slippers as the first are centered while the second are off-centered (and thus see a lower flow velocity) [3].

Figure S2 depicts the corresponding simulation setups, which are identical to the one from the main text except for the different RBC shape. Especially note that the initial radial offset r_{init} of the centroid is along the same line. We always use the same croissant or slipper shape, regardless of the value of r_{init}.

The slipper and croissant shapes represent the "extreme" cases, as the steady state consists of slippers and croissants and thus by starting with the respective shape one expects to "manipulate" the cells into these particular shapes. The discocyte shape represents the equilibrium shape assumed by RBCs without external forces and is thus another natural starting point.

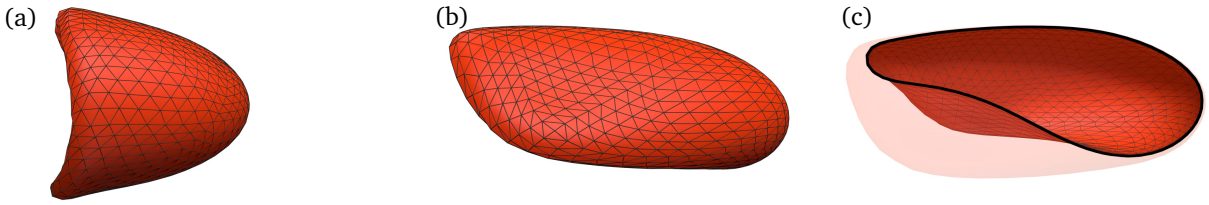

Figure S1: Employed initial shapes in the simulations when starting as a (a) croissant or (b) slipper. Figure (c) shows the cross-section of the slipper from (b). The black lines on the surfaces represent the used mesh.

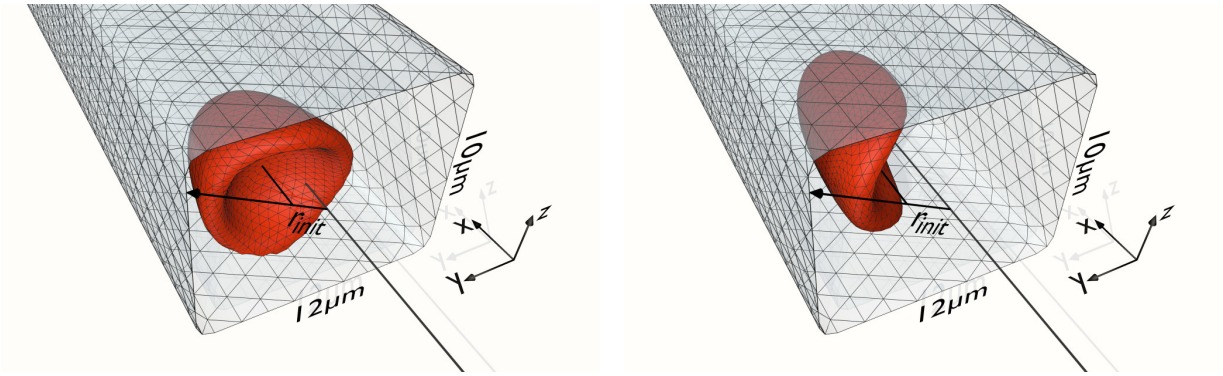

Figure S2: The simulation setups when starting with a croissant (left) or a slipper shape (right), similar to figure 2 from the main text. The cell shapes are the ones from figure S1.

S1.2 Starting with rotated discocytes

When we start with the discocyte shape in the main text, it is axis-aligned with the channel's axis (x-axis; see figure 2 in the main text). A natural question that occurs is thus how the results change if the rotation is varied. We therefore present in figure S3 phase diagrams when the symmetry axis of the initial discocyte is aligned with the y-axis (a) or z-axis (b).

Compared to the results from the main text, we observe that many more of the final shapes are croissants, even for high initial radial positions r_{init} that resulted in slippers for our main starting shapes (croissant, slipper, x-aligned discocyte). Considering the time evolution of the radial position (exemplified in figure S4), we find that the rotated discocytes are quickly pushed into the center of the channel before sufficient deformations can occur that would induce a slipper as the final state. In other words, the initial transient of these initial shapes happens to favor croissants. A more detailed analysis of this behavior and the underlying reason will be left for future research.

Some of the experimental recordings at the channel entrance (see section S7) appear to be somewhat similar to z-aligned discocytes. However, as we almost only find croissants in the steady state for this particular starting shape in the simulations (figure S3(b)), contrary to the actually observed domination of slippers in the steady state in the experiments (figure 3(a) in the main text), it is likely that many of these cells at the channel entrance

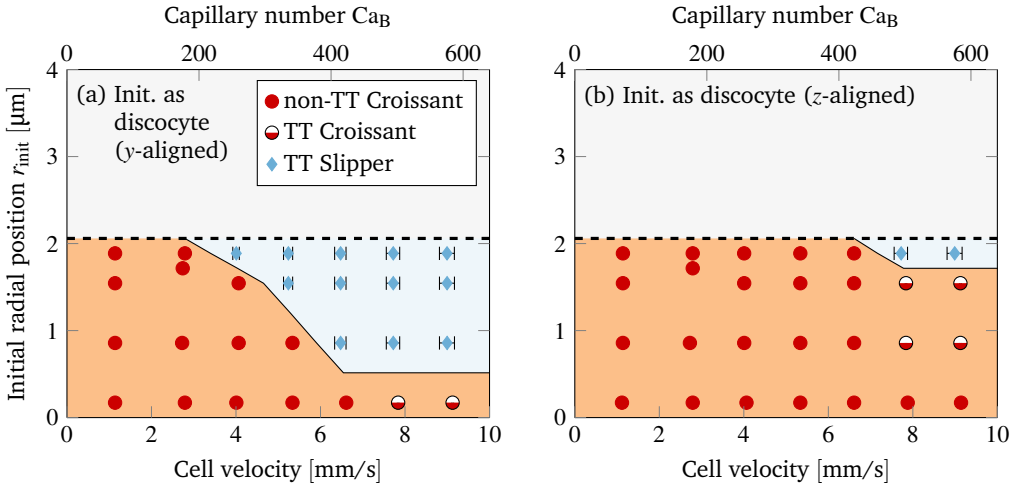

Figure S3: Phase diagrams obtained from the simulations when starting with the typical discocyte shape which is aligned with (a) the y-axis and (b) the z-axis. Figure elements as in figure 6 in the main text.

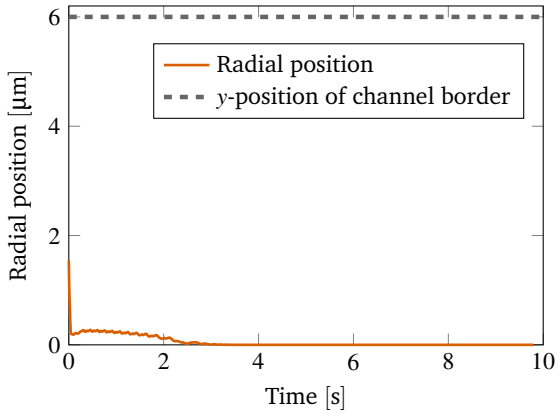

Figure S4: Radial position of an RBC started in the typical discocyte shape that is aligned along the z-axis with a radial offset of $r_{init} \approx 1.54\,\mu m$. It has a cell velocity of approximately 6.61 mm/s in the steady state. The initial transient quickly pushes the cell to the center of the channel, where it becomes a croissant.

are actually not discocytes but rather deformed shapes, such as slippers viewed from the top or "edge-on" discocytes [4].

S2 Time evolution and steady state details

As noted in the main text and shown in the `TTSlipper` supplementary video, the tank-treading (TT) slipper exhibits oscillatory contractions. These result in periodic variations of the radial position and the cell velocity, as exemplified in figure S5. This figure also illustrates how we extract the average, minimal and maximal values after reaching the steady state. The simulation results from the main text depict the average values as the main data points and the minimal and maximal values via error bars. Note that we do the same for the other shapes, although the resulting error bars are too small to be seen in the figures.

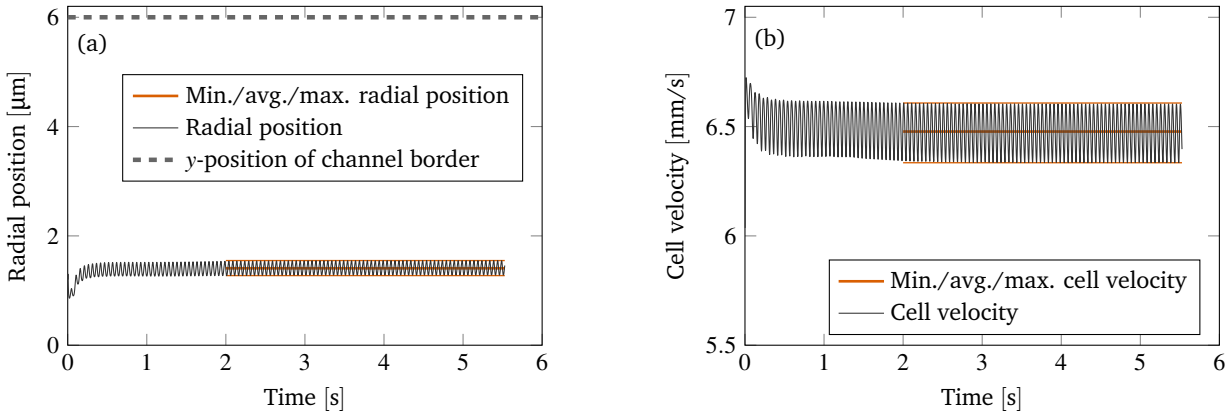

Figure S5: Time evolution of (a) the radial position and (b) the cell velocity for a slipper shape. The data is for the numerical simulation with $r_{\text{init}} = 1.2\,\mu\text{m}$ from figure 5 in the main text. The orange lines show from bottom to top the minimum, average and maximum values that are extracted in the steady state, which is taken to begin at 2 s in this particular example.

Furthermore, reaching the steady state often takes a few seconds. Convergence into the croissant shape usually takes longer than reaching a steady slipper state. This is illustrated in figure S6(a) where we show for each simulation from figure 6 in the main text the approximated time t_{steady} until the steady state is reached. This time t_{steady} is the duration measured from the start of the simulations until the position, shape, velocity and asphericity (a measure of deformation [5]) of the cells no longer change or become periodic. Figure S6(b) shows the same times non-dimensionalized with a typical flow timescale $\tau := R_{\text{RBC}}/u$, where u is the mean cell velocity.

The longest times are observed when the velocity lies in the croissant-only range. An example for such a case is displayed in figure S7: For around eight seconds, the cell is in an almost periodic slipper state before moving to the center and becoming a croissant. However, after another four seconds some membrane rotation occurs, i.e. the RBC dimples (which are special points due to the discocyte reference state) move to a slightly different location. This results in a short lived and slightly off-centered position. After a total time of around 14 s the cell is in the final croissant state, with no movement occurring anymore. See the video `LongCroissant` for an illustration.

Regarding a more quantitative measure for the steady state: Within a time frame spanning several oscillations or a time frame of 1000τ measured from the beginning of the steady state (t_{steady}), the changes are approximately

- below 2 % for the radial position (even below 0.2 % for $u > 0.8\,\text{mm/s}$; relative to R_{RBC}),
- below 1 % for the cell velocity (even below 0.1 % for $u > 0.8\,\text{mm/s}$; relative to the average cell velocity u) and
- below 1 % for the asphericity (relative to the average asphericity).

For periodic motion, the maxima/minima within the time frame are considered.

It is important to note that the times reported here are the times until the cell shapes have entirely converged. The rough cell shape (TT/non-TT croissant or TT/non-TT slipper) are usually apparent much earlier. For

example, in figures S5 the slipper can be recognized even before 1 s, while the perfectly periodic state is reached only after 2 s. Another example is figure S7, where we find a croissant already at approximately 9 s, and only minor differences occur compared to the fully converged state at 14 s. Considering the times until the rough cell shape is apparent together with the cell velocities, we find that in the overwhelming majority of cases the cells have traveled for less than 10 mm before the rough cell shape is attained. This is in agreement with our choice of measurement position in the experiments (10 mm away from the channel entrance).

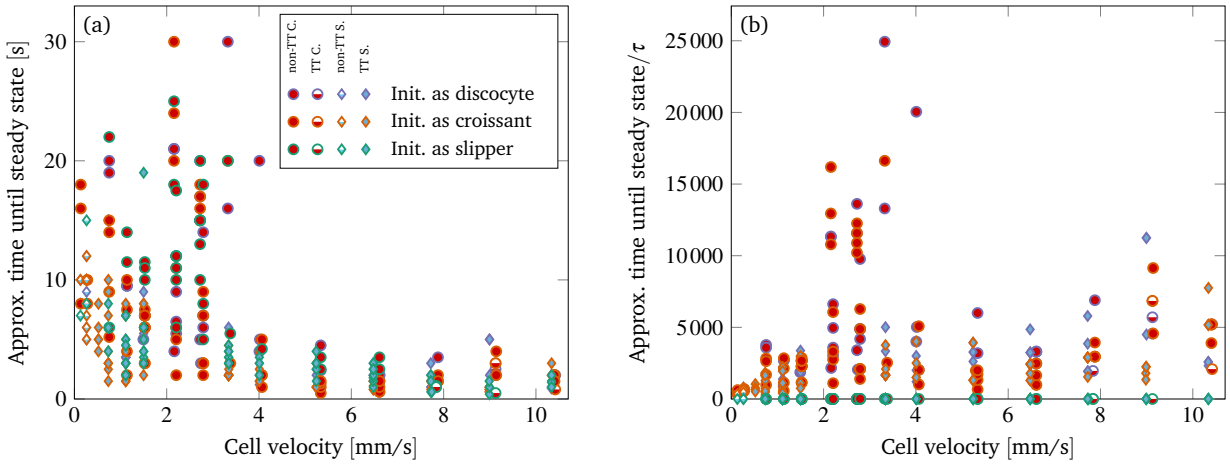

Figure S6: Estimates of the time t_{steady} it takes for the cells to reach the steady state. Figure (a) depicts this time in seconds, while figure (b) shows the time non-dimensionalized with a typical flow timescale τ. The images show the results for all simulations from the three diagrams from figure 6 in the main text, where the cell was initialized as x-aligned discocyte, croissant and slipper, respectively. These three initial shapes are indicated by the purple, orange and green borders around the symbols (see the three rows in the legend). The final steady state shapes (non-tank-treading croissant, tank-treading croissant, non-tank-treading slipper and tank-treading slipper) are represented by the same symbols as in the main text (compare the four columns in the legend).

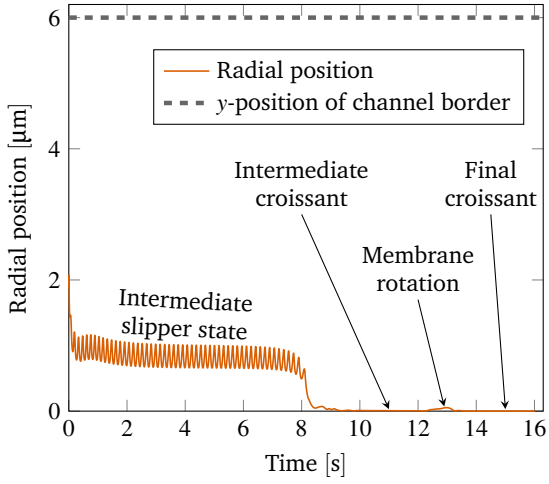

Figure S7: Time evolution of the radial position of a cell which is initially in the x-aligned discocyte state with $r_{\text{init}} \approx 1.89\,\mu\text{m}$ and has an average velocity of $\approx 2.79\,\text{mm/s}$ in the steady state (i.e. it lies in the croissant-only region). The steady state begins at around 14 s. See the movie `LongCroissant` for a 3D visualization.

S3 About the error bars in the prediction

The determination of the vertical error bars in the comparison between experiments and simulations (figure 8 in the main text) consists of several steps that will be described in the following. To this end, consider figure S8. This figure shows exemplarily the numerical phase diagram when the starting shape is the x-aligned discocyte, i.e. the symbols that indicate the steady states are identical to figure 6(a) from the main text. The middle gray line represents the position of the approximated transition threshold r_{trans} between croissants and slippers, which was obtained by averaging the values from the adjacent simulation symbols.

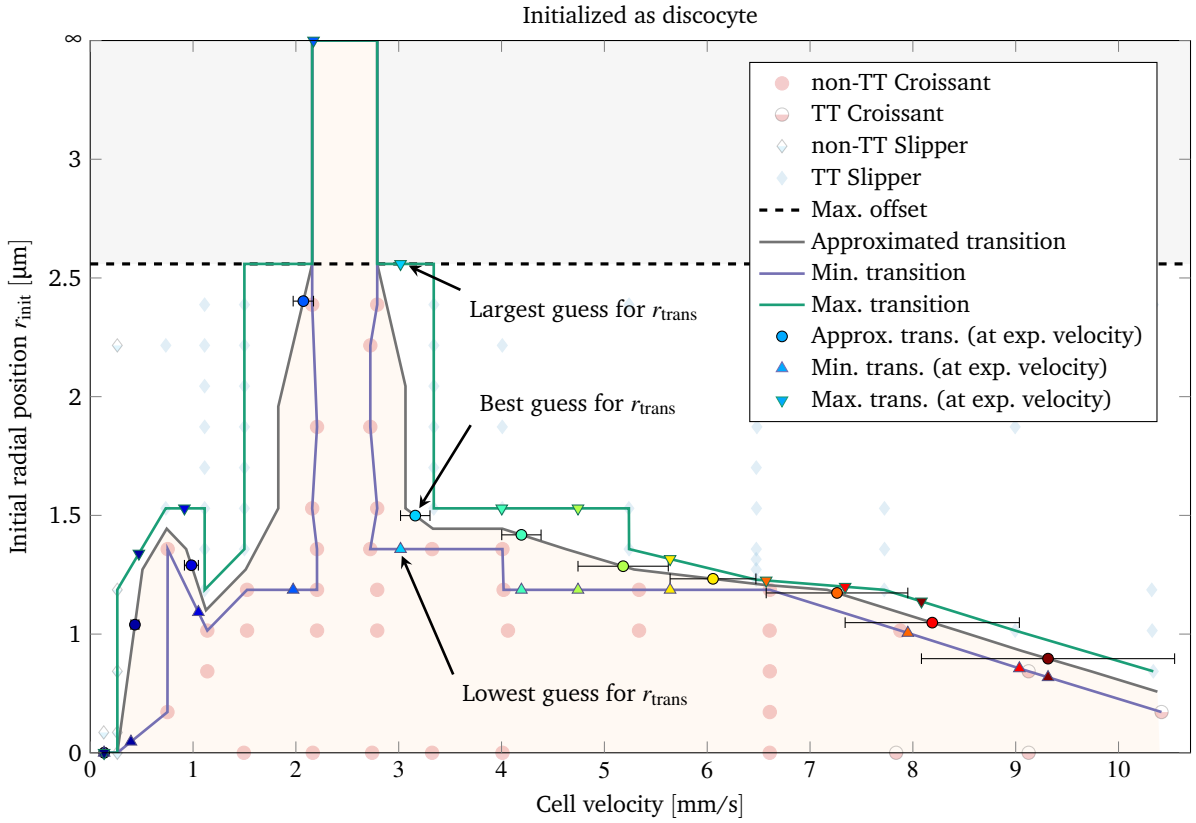

Figure S8: Numerical phase diagram from figure 6(a) from the main text for the x-aligned discocyte starting shape. The nearly transparent shape symbols and the maximal offset are identical to figure 6(a). The violet, gray and green lines depict the minimal, average and maximal position, respectively, of the transition threshold r_{trans} between croissants and slippers. These lines are evaluated at the experimental velocities u and $u \pm \sigma_u$, giving the circular and triangular symbols. Each triple of these symbols that shares the same color corresponds to one particular experimental velocity and shows the lowest, best and largest guess for r_{trans}. This is exemplified via the three labels and arrows for $u \pm \sigma_u = (3.16 \pm 0.14)\,\text{mm/s}$ which corresponds to a pressure drop of $\Delta P = 300\,\text{mbar}$. The horizontal error bars depict σ_u. Also note that in the croissant-only region we take $r_{\text{trans}} \to \infty$, as indicated by the ∞ symbol on the top left.

The first step in the determination of the vertical error bars is to compute a lower and upper bound for the transition threshold. We do this by drawing a line through the highest croissant and lowest slipper symbols. This leads to the lower violet and upper green lines in figure S8. Thus, these two lines represent the uncertainty of the transition, which is a result of the finite distance between the simulations.

An exception in the construction of the three lines occurs in the region where the simulations predict only croissants. Due to the particular starting shape, there is a maximal initial offset. Experimentally, however, it is of course possible that the cells at the channel entrance have a larger offset (i.e. one that lies above the black dashed line in figure S8). Since the results from the simulations indicate that only croissants really exist in this region (regardless of the initial shape and offset), we take $r_{\text{trans}} \to \infty$. That way we predict a value of 1 for the fraction of croissants.

Second, we need to evaluate the transition lines at the experimental velocities. However, the measured velocities have not only an average u but also a certain standard deviation σ_u. σ_u is taken as the uncertainty in the velocity here. Evaluating the middle gray line at the average velocity u results in the "best guess for r_{trans}" (the circular symbols in figure S8). This value is then directly converted into the predicted fraction of croissants ϕ as described in the main text (via conversion to y_{trans} and the measured offset distribution at the channel entrance). For the vertical error bars, we evaluate the three numerical transition lines (lower, middle and upper, i.e. violet, gray and green) at the three velocities u, $u-\sigma_u$ and $u+\sigma_u$, leading to nine values for r_{trans}. The ones that will yield the lowest and largest fraction of croissants are shown as triangular symbols in figure S8 (the "lowest guess for r_{trans}" and the "largest guess for r_{trans}").

Third, the predicted fractions of croissants are computed from the offset distribution at the channel entrance for each of these nine r_{trans} values (as described in the main text), and additionally for $r_{\text{trans}} \pm s_{\text{P}}$. This takes into account the uncertainty in the offset distribution due to the uncertainty s_{P} in the position measurement. As a result, we now have 27 predictions.

Fourth, we search for the minimum (ϕ_{min}) and maximum (ϕ_{max}) of these 27 values. ϕ_{min} and ϕ_{max} are then interpreted as the uncertainty in the prediction. The vertical error bars in figure 8 from the main text therefore depict ϕ_{min} and ϕ_{max}.

All of this is performed not only for the phase diagram with the discocyte, but also for the ones with the croissant and slipper starting shapes. In case of the croissant starting shape, r_{trans} is not a proper function due to the protrusions, i.e. we find several transition offsets for certain velocities (compare figure 6(b) in the main text). Hence, the simple "counting of cells that enter with an offset below r_{trans}" to form the prediction becomes a "counting of cells that enter with offsets in the intervals formed by the numerical transition offsets". As an example, if a certain velocity leads to transitions at r_1, r_2 and r_3 (such that the simulations yield croissants in the two intervals $[0, r_1]$ and $[r_2, r_3]$), then we count how many cells enter the channel with offsets that lie in these two intervals (after their projection on the y-axis). The computation of the uncertainty is adapted accordingly.

S4 Supplementary information for the experiments

S4.1 Inlet in the experimental setup

Figure S9 depicts part of the inlet reservoir and the start of the channels. The whole chip is made of PDMS. The total reservoir is rectangular with a length of 4 mm and a width of 1 mm. Multiple channels are connected to this reservoir, having a width of $L_y \approx 12\,\mu\text{m}$ and a height of $L_z \approx 10\,\mu\text{m}$. Using our microscope, we record several channels simultaneously to increase the throughput.

To connect the reservoir with our high-precision pressure device, we pinch a hole into the PDMS substrate. Its diameter is approximately 1 mm, matching with the diameter of the connected tube. In the example in figure S9 the flow together with the RBCs is coming from the top. The RBCs then flow into the channels since the outlet is at the end of them. The outlet reservoir looks similar. Also note that the distribution of the RBCs before the channel entrances is without significance for the present work since we record the actual state directly beyond the entrance, effectively *defining* it as the initial condition in the experiments (see below for the shapes and figure 4 in the main text).

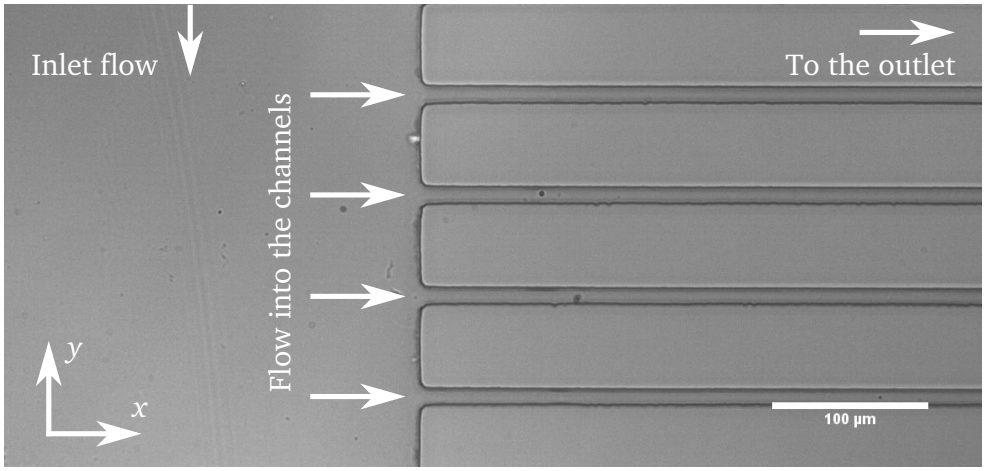

Figure S9: Part of the channel inlet used in the experiments. Top-view, i.e. gravity is going into the image plane (z-direction). Note that the total length of the channels is $L_x \approx 40\,\text{mm}$, i.e. only the entry part is shown here.

S4.2 Additional experimental data

We depict in figure S10 the measured cell velocities for each applied pressure drop ΔP. The data shows the result when the averaging goes over all cells regardless of their shape ("All"), and also for the three shape classes separately. Obviously, the cell velocities are roughly proportional to ΔP. However, croissants tend to be a bit faster than slippers because croissants are located in the high-velocity center of the channel while slippers are off-centered (see the main text). This is in agreement with previous publications [3, 6].

Table S1 lists the corresponding raw data, as well as the number of cells that were taken into account. It additionally shows the number of cells at the channel entrance. The raw images from the experiments are included in sections S6 and S7 below.

Furthermore, we list in an extra Excel sheet (`SI_rawYPos_pos0.xls`) the raw y-positions of the cells at the channel entrance. This data makes it possible to compare one's own simulation results with our experiments (as we did in figure 8 in the main text).

Moreover, figure S11 depicts the experimental y-offset distributions separated into the contributions from the three different shapes (croissants, slippers and "others") at position $x = 10\,\text{mm}$ in the channel. This figure complements figure 3(b) from the main text where all three shapes have been considered together.

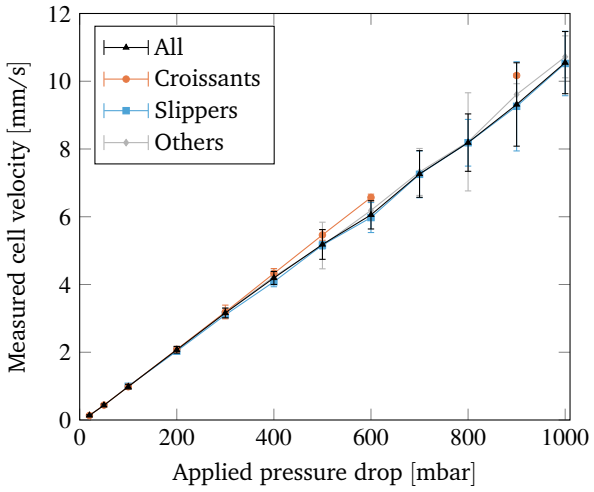

Figure S10: Measured average cell velocities for each applied pressure drop for the three different shape classes and once for all shapes together ("All"). The vertical error bars depict the standard deviation σ_u. Measurements were performed at position $x = 10\,\text{mm}$ in the channel. The corresponding raw data is listed in table S1. The lines are guides for the eyes.

ΔP [mbar]	N_0^{all}	N_{10}^{all}	N_{10}^{Crois}	N_{10}^{Slipper}	N_{10}^{Other}	u_{10}^{all} [mm/s]	u_{10}^{Crois} [mm/s]	u_{10}^{Slipper} [mm/s]	u_{10}^{Other} [mm/s]
20	35	107	9	0	98	0.135 ± 0.021	0.132 ± 0.020		0.135 ± 0.021
50	10	52	9	0	43	0.43 ± 0.04	0.440 ± 0.005		0.43 ± 0.04
100	29	205	165	2	38	0.98 ± 0.07	0.98 ± 0.07	0.996 ± 0.002	0.99 ± 0.04
200	71	484	252	22	210	2.07 ± 0.10	2.09 ± 0.08	2.03 ± 0.06	2.06 ± 0.12
300	95	475	102	120	253	3.16 ± 0.14	3.19 ± 0.20	3.10 ± 0.09	3.18 ± 0.13
400	90	463	80	167	216	4.19 ± 0.19	4.33 ± 0.14	4.08 ± 0.15	4.23 ± 0.19
500	179	215	17	117	81	5.2 ± 0.4	5.46 ± 0.16	5.16 ± 0.11	5.2 ± 0.7
600	151	176	8	124	44	6.1 ± 0.4	6.57 ± 0.10	6.0 ± 0.4	6.19 ± 0.25
700	159	123	0	105	18	7.3 ± 0.7		7.3 ± 0.7	7.3 ± 0.7
800	75	200	0	169	31	8.2 ± 0.8		8.2 ± 0.7	8.21 ± 1.40
900	187	282	2	241	39	9.3 ± 1.2	10.17 ± 0.06	9.3 ± 1.3	9.6 ± 0.3
1000	141	305	0	266	39	10.6 ± 0.9		10.5 ± 1.0	10.7 ± 0.6

Table S1: Experimental data: The table lists for each applied pressure drop ΔP the total number of analyzed cells N_0^{all} at position $x = 0\,\text{mm}$ in the channel and the total number of analyzed cells N_{10}^{all} at position $x = 10\,\text{mm}$. For the latter we also show the number of croissants, slippers and "others", together with the measured velocities u_{10}. The uncertainties are the standard deviation. The subscripts "0" and "10" in the heading specify the x-position in the channel (0 mm or 10 mm).

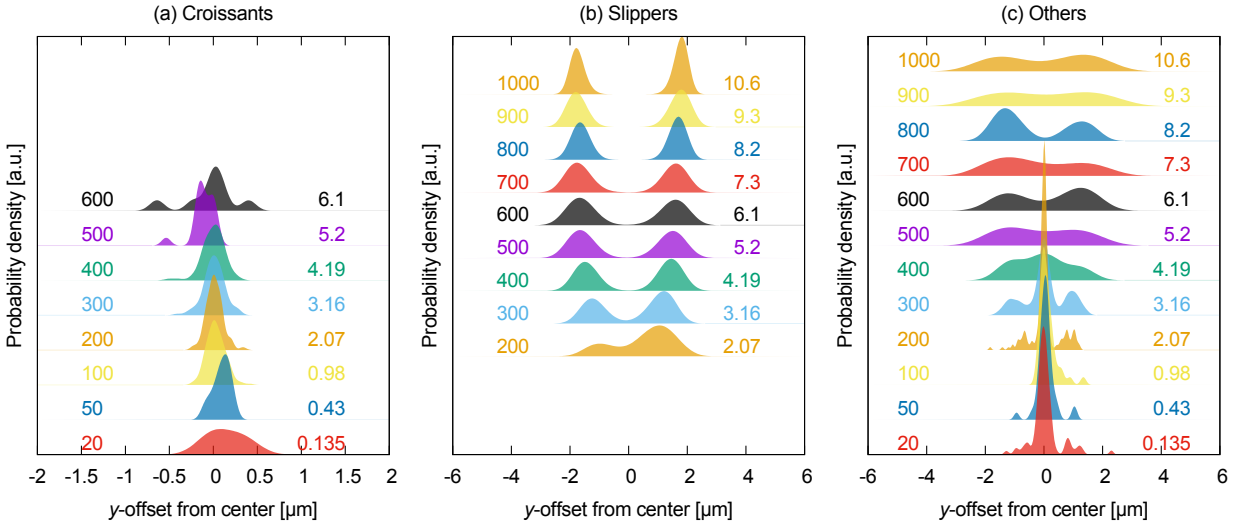

Figure S11: Estimated probability density functions for the experimental y-offset distributions at position $x = 10\,\text{mm}$ in the channel for (a) the croissant, (b) the slipper and (c) the "other" shapes. The result for all three shapes combined was shown in figure 3(b) in the main text. The area below each curve is normalized to 1, and they are offset in the vertical direction for illustration purposes. The applied pressure drop is indicate on the left side of the figures in millibars, while the corresponding mean cell velocity is shown on the right side in mm/s. Also note the different scale of the horizontal axis in the first figure.

S5 References

[1] E. Evans and Y.-C. Fung, *"Improved measurements of the erythrocyte geometry,"* Microvasc. Res. **4**, 335 (1972).

[2] D.-V. Le, *"Subdivision elements for large deformation of liquid capsules enclosed by thin shells,"* Comput. Methods Appl. Mech. Eng. **199**, 2622 (2010).

[3] S. Quint, A. F. Christ, A. Guckenberger, S. Himbert, L. Kaestner, S. Gekle, and C. Wagner, *"3D tomography of cells in micro-channels,"* Appl. Phys. Lett. **111**, 103701 (2017).

[4] R. Skalak and P. I. Branemark, *"Deformation of Red Blood Cells in Capillaries,"* Science **164**, 717 (1969).

[5] D. A. Fedosov, M. Peltomäki, and G. Gompper, *"Deformation and dynamics of red blood cells in flow through cylindrical microchannels,"* Soft Matter **10**, 4258 (2014).

[6] G. Tomaiuolo, M. Simeone, V. Martinelli, B. Rotoli, and S. Guido, *"Red blood cell deformation in microconfined flow,"* Soft Matter **5**, 3736 (2009).

S6 Raw experimental images at $x = 10\,\mathrm{mm}$

Note: The images in the individual collections are ordered from centered to off-centered.
Note: Many of the "others" (e.g. for $\Delta P = 200\,\mathrm{mbar}$) might be croissants, but they can also be slippers that are viewed from the "top" (i.e. when camera would point along the z-direction, one might see slippers). Since we cannot decide this from these images, we classify them as "others".

$\Delta P = 20\,\mathrm{mbar}$, $x = 10\,\mathrm{mm}$

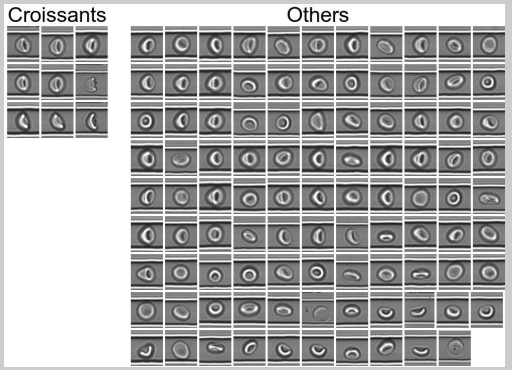

$\Delta P = 50\,\mathrm{mbar}$, $x = 10\,\mathrm{mm}$

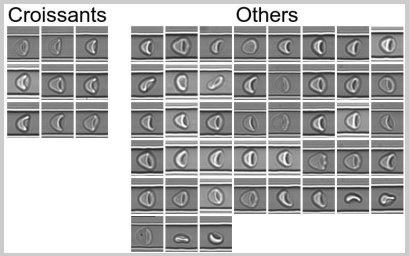

$\Delta P = 100\,\mathrm{mbar}$, $x = 10\,\mathrm{mm}$

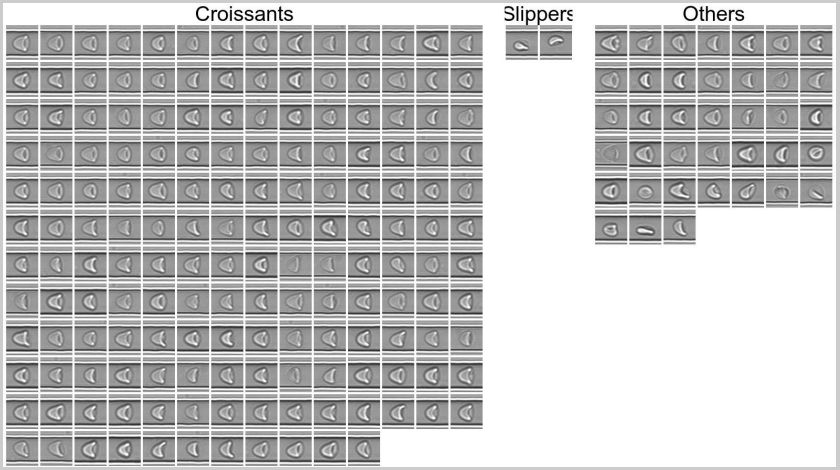

$\Delta P = 200\,\text{mbar},\ x = 10\,\text{mm}$

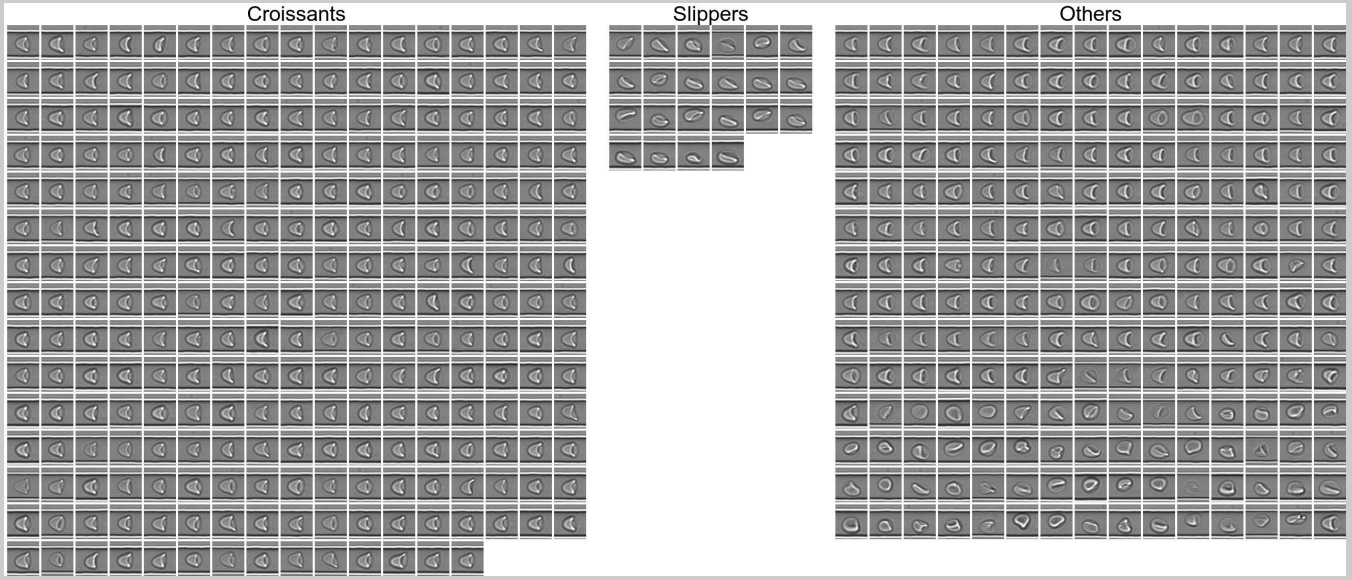

$\Delta P = 300\,\text{mbar},\ x = 10\,\text{mm}$

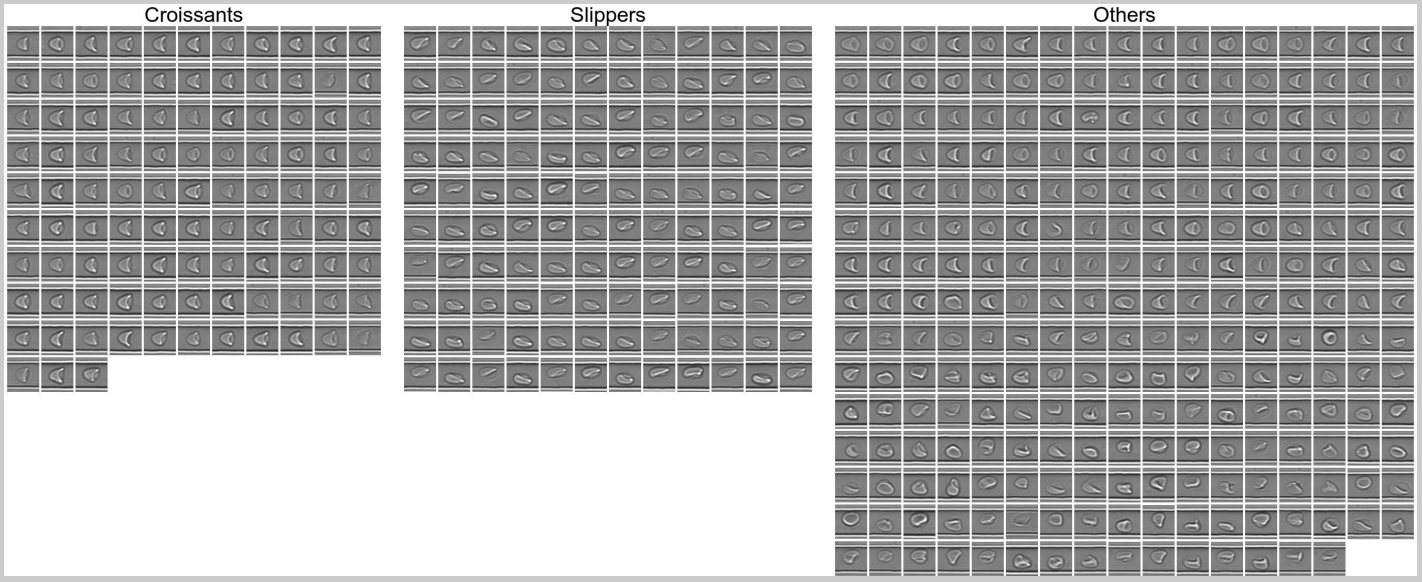

$\Delta P = 400\,\text{mbar},\ x = 10\,\text{mm}$

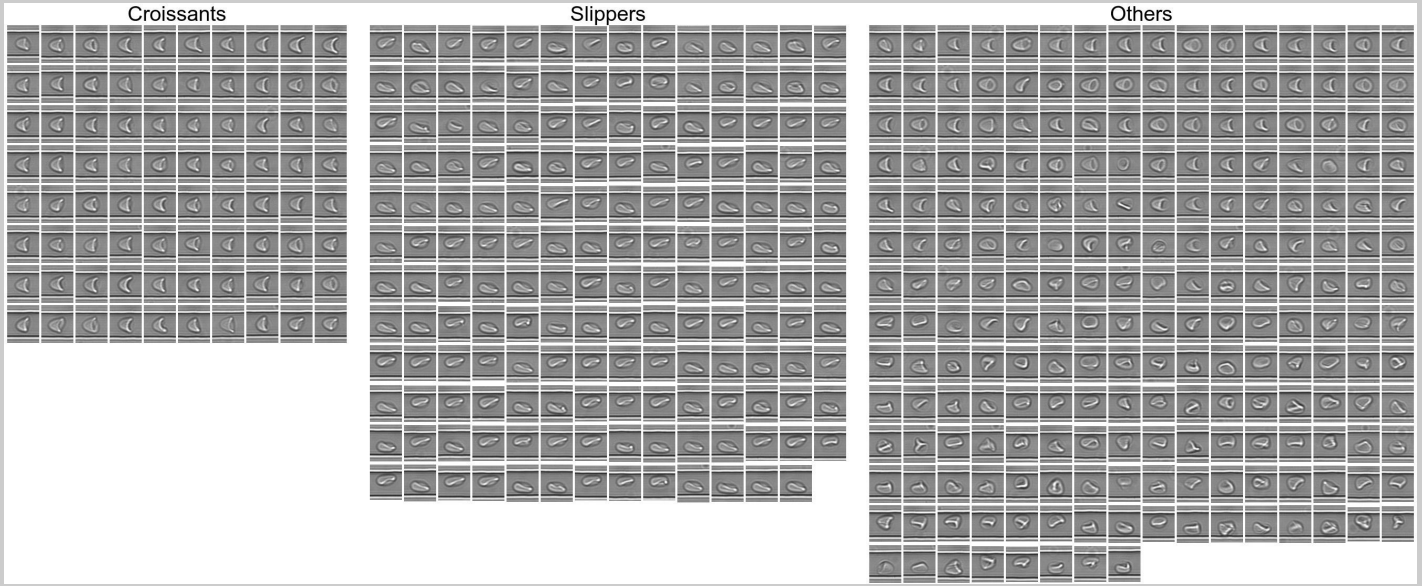

$\Delta P = 500\,\text{mbar},\ x = 10\,\text{mm}$

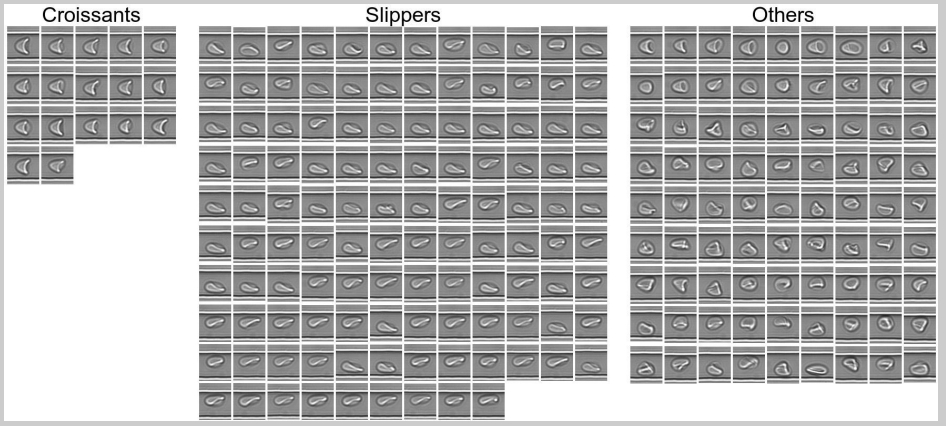

$\Delta P = 600\,\text{mbar},\ x = 10\,\text{mm}$

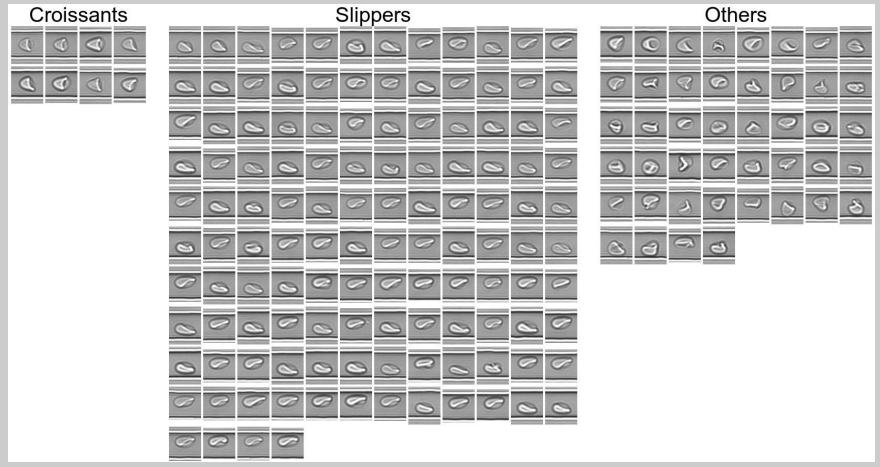

$\Delta P = 700\,\text{mbar},\ x = 10\,\text{mm}$

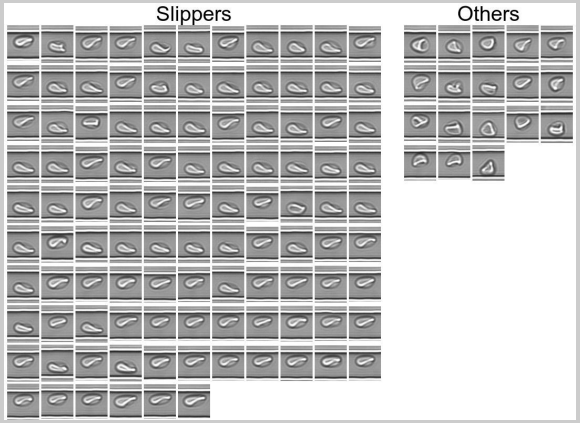

$\Delta P = 800\,\text{mbar},\ x = 10\,\text{mm}$

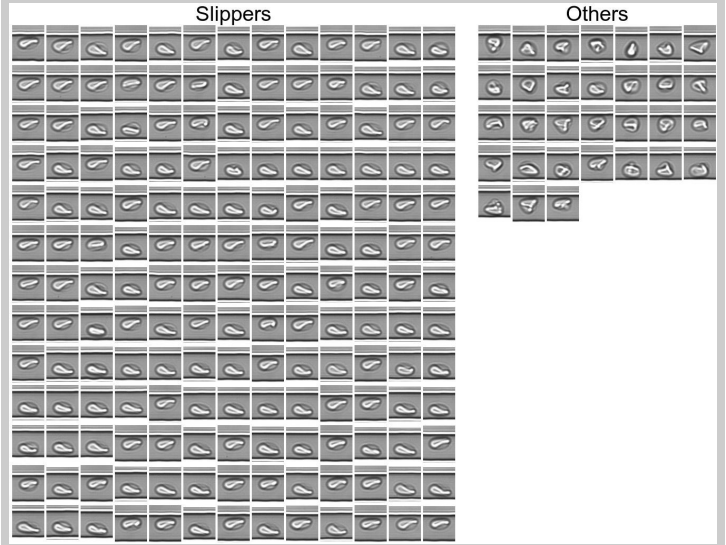

$\Delta P = 900\,\text{mbar}$, $x = 10\,\text{mm}$

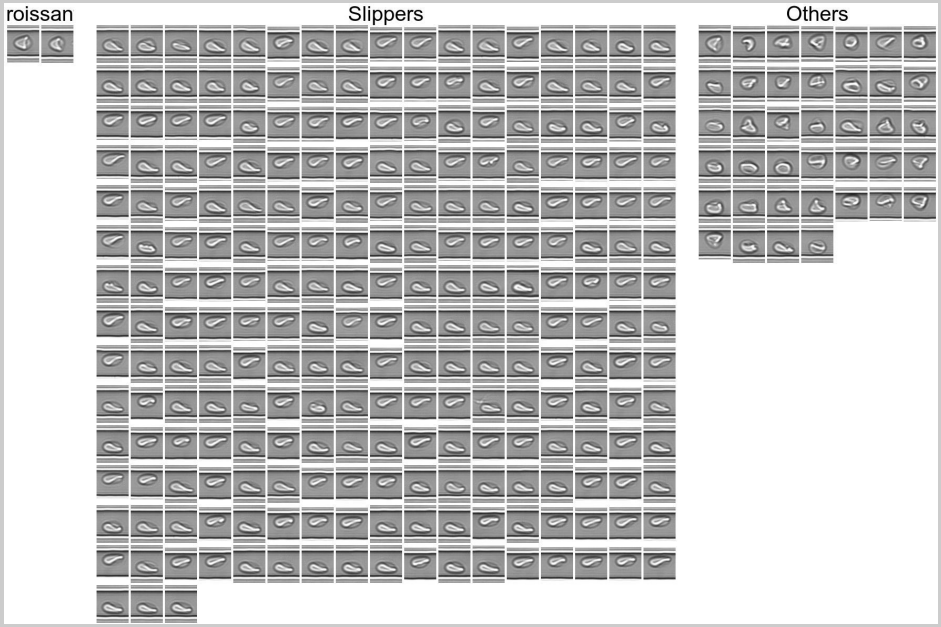

$\Delta P = 1000\,\text{mbar}$, $x = 10\,\text{mm}$

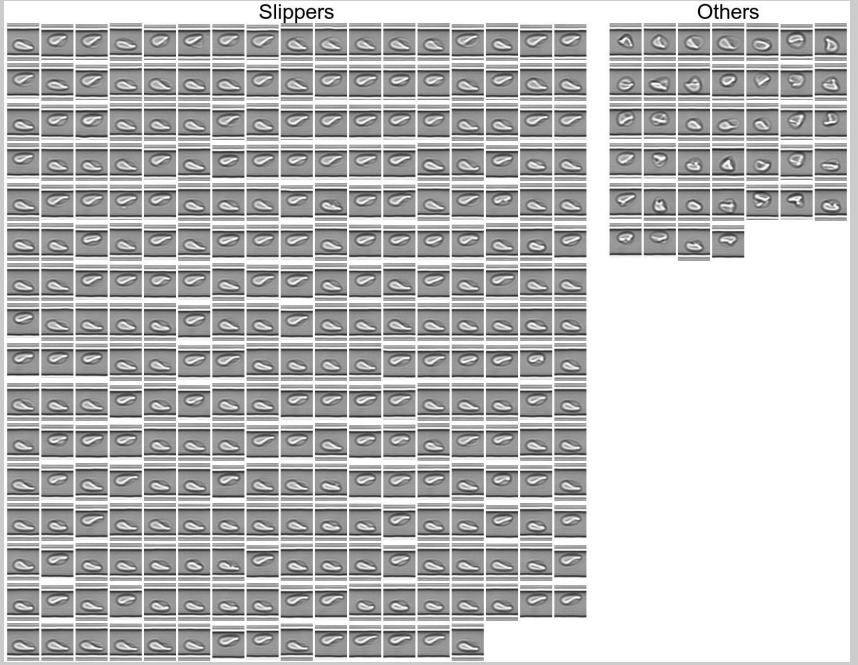

S7 Raw experimental images at $x = 0\,\mathrm{mm}$

Note: The images in the individual collections are ordered from centered to off-centered.

$\Delta P = 20\,\mathrm{mbar}$, $x = 0\,\mathrm{mm}$

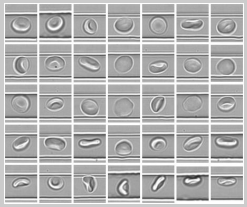

$\Delta P = 50\,\mathrm{mbar}$, $x = 0\,\mathrm{mm}$

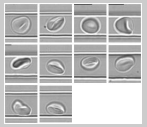

$\Delta P = 100\,\mathrm{mbar}$, $x = 0\,\mathrm{mm}$

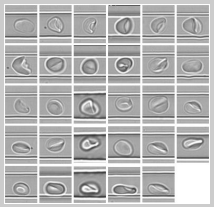

$\Delta P = 200\,\mathrm{mbar}$, $x = 0\,\mathrm{mm}$

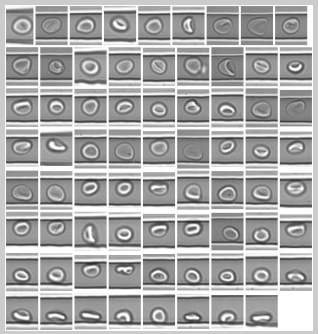

$\Delta P = 300\,\mathrm{mbar}$, $x = 0\,\mathrm{mm}$

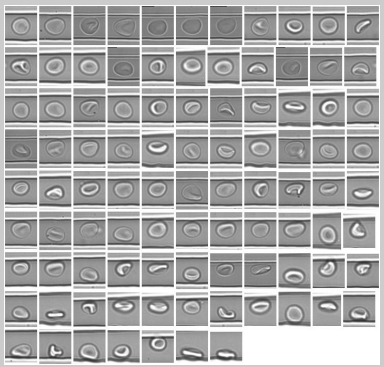

$\Delta P = 400\,\mathrm{mbar}$, $x = 0\,\mathrm{mm}$

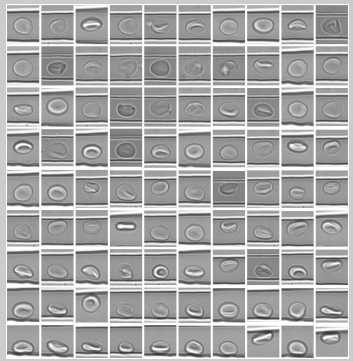

$\Delta P = 500\,\mathrm{mbar}$, $x = 0\,\mathrm{mm}$

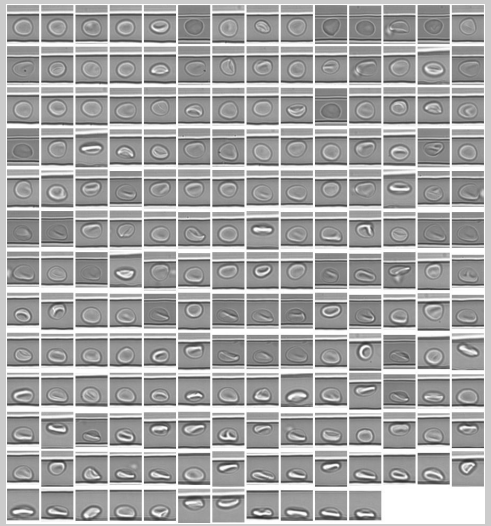

$\Delta P = 600\,\text{mbar},\ x = 0\,\text{mm}$

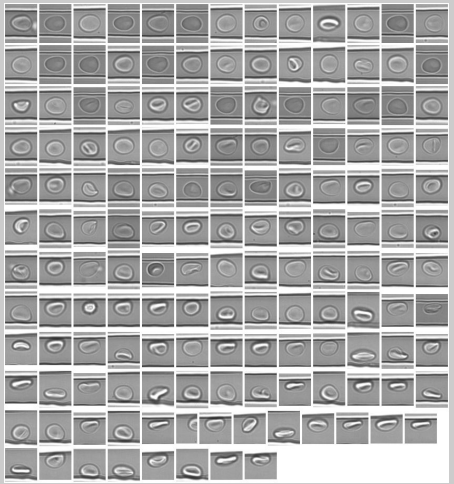

$\Delta P = 700\,\text{mbar},\ x = 0\,\text{mm}$

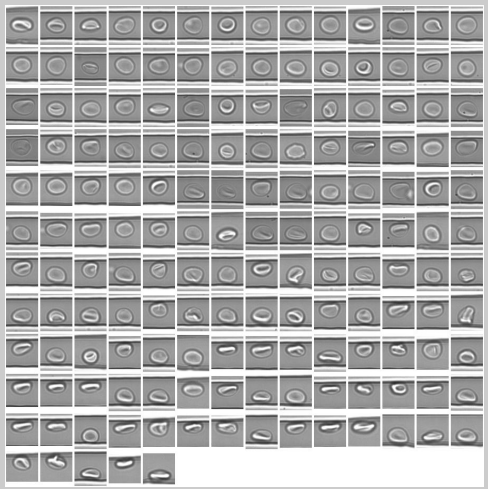

$\Delta P = 800\,\text{mbar},\ x = 0\,\text{mm}$

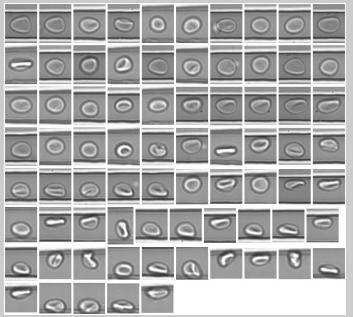

$\Delta P = 900\,\text{mbar},\ x = 0\,\text{mm}$

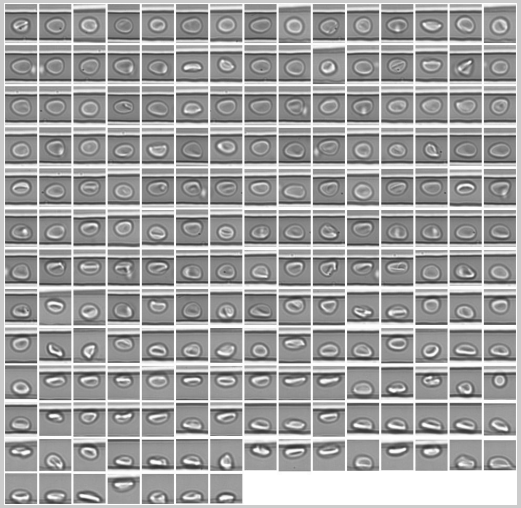

$\Delta P = 1000\,\text{mbar},\ x = 0\,\text{mm}$